



Free-standing flexible graphene oxide paper electrode for rechargeable Li–O₂ batteries

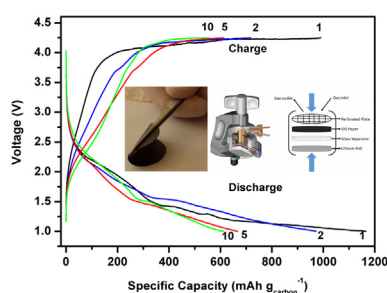
Tugrul Cetinkaya*, Seyma Ozcan, Mehmet Uysal, Mehmet O. Guler, Hatem Akbulut

Sakarya University, Engineering Faculty, Department of Metallurgical & Materials Engineering, Esentepe Campus, 54187 Sakarya, Turkey

HIGHLIGHTS

- A novel graphene oxide paper was produced by vacuum filtration technique.
- The graphene oxide paper was used as air breathing cathode for Li–O₂ batteries.
- The GO paper exhibited a 612 mAh g^{−1} discharge capacity and a 585 mAh g^{−1} charge capacity after 10 cycles.

GRAPHICAL ABSTRACT



ARTICLE INFO

Article history:

Received 26 December 2013

Received in revised form

5 April 2014

Accepted 15 May 2014

Available online 24 May 2014

Keywords:

Graphene oxide

Cathode

Li–O₂ batteries

Electrochemical cycling

EIS

ABSTRACT

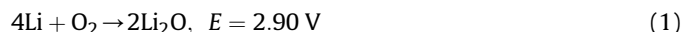
A smooth, free-standing and flexible graphene oxide paper was produced using a vacuum filtration technique. This graphene oxide paper was characterized by scanning electron microscopy, X-ray diffraction and Raman spectroscopy techniques. The charge–discharge characteristics of the graphene oxide paper have been investigated from 1 V to 4.5 V at a constant 0.01 mA cm^{−2} with an ECC–Air test cell. The electrochemical impedance of the graphene oxide paper has been measured to investigate the difference in the resistance of the cell before and after an electrochemical cycling test. The Li–air cell with a graphene oxide flexible paper cathode exhibited a 612 mAh g^{−1} discharge capacity and a 555 mAh g^{−1} charge capacity after 10 cycles. This study demonstrated that graphene oxide paper might be a good alternative cathode material for Li–O₂ batteries in the future.

© 2014 Elsevier B.V. All rights reserved.

1. Introduction

Breakthroughs in battery science and technology have become increasingly necessary to power the needs of modern society due to the growing concerns over fossil fuel depletion and climate change [1,2]. Currently, battery research and development have focused on energy storage and conversion with high energy, high power density, and reliable safety [3]. Among batteries, the lithium–air battery has recently captured worldwide attention due to its

ultrahigh specific energy density of 11.140 Wh kg^{−1}, rivaling that of gasoline [4]. A typical non-aqueous lithium–air battery consists of a metallic lithium anode, an electrolyte with a lithium salt dissolved in an aprotic solvent and a porous O₂-breathing cathode [5]. The air electrode (positive electrode) is the important battery component upon which the discharge products (LiO_x) are deposited and/or decomposed as described by the following cell reactions (discharge) [6]:



* Corresponding author. Tel.: +90 555 6233694; fax: +90 264 2955601.

E-mail addresses: tcetinkaya@sakarya.edu.tr, tugrulcetinkaya@gmail.com (T. Cetinkaya).

The reverse of Reactions (1) and (2) reveal that the oxygen gas evolution causes the charge process.

However, despite the extensive research effort devoted to its practical implementation, several issues with the electrodes and electrolytes have limited the performance of lithium–air batteries to a few charge–discharge cycles and a low rate capability [7]. Therefore, an extremely effective carbon cathode for high performance Li–O₂ batteries must be designed and produced. For this aim, much research has focused on the different types of carbon-based air-breathing cathodes using high surface area carbons [8], carbon nanotubes [9] carbon nanotube/carbon nanofiber bucky-papers [10,11], aerogel carbon [12], diamond-like carbon [5] and graphene [13]. Consequently, the capacity of the oxygen electrode depends on the surface area of the large pores. Therefore, a carbon material with a high pore volume and a large pore diameter could exhibit an increased discharge capacity [12,14]. However, a binder is used on the cathode, promoting aggregation of the carbon particles; this aggregation leads to low O₂ diffusion rates and provides limited space for Li₂O₂ deposition due to the preparation of the carbon air-breathing cathode.

Graphene oxide (GO) consists of a two-dimensional (2D) sheet of covalently bonded carbon atoms bearing various oxygen functional groups (e.g., hydroxyl, epoxide, and carbonyl groups) on their basal planes and edges. The as-formed GO paper consists of interlocked/tiled GO nanosheets; this structure imparts a high mechanical stiffness and strength compared to other paper-like membrane materials [15,16]. Therefore, GO paper has been used in many applications, such as polymer electrolyte fuel cells (PEMFCs) [17], cellular imaging and drug delivery [18]. Recently, a GO gel-derived free-standing electrode was prepared by Wang et al. [14] for a high rate Li–O₂ battery; this material displayed a high capacity and a high rate performance, demonstrating that GO is a highly efficient oxygen electrode material for Li–O₂ batteries.

We report a smooth, free-standing and flexible GO paper produced by a vacuum filtration technique for use as a lithium air-breathing cathode material without using any binder or additives in Li–O₂ batteries. Although, GO paper has been used in many different fields, this study is the first to use GO paper as a lithium air-breathing cathode for Li–O₂ batteries. GO paper provides a highly efficient capacity and reversible reaction due to the stable, flexible and porous nature of the GO paper.

2. Experimental details

2.1. Preparation of graphite oxide

Graphite oxide was obtained from graphite flakes (Alfa Aesar, +100 mesh in size) using the method described by Hummers [19]. The graphite particles were pretreated to activate the surface of the graphite flakes, facilitating the exfoliation of the van der Waals bonds between the graphene layers. The graphite flakes

were dispersed in 50 ml of a solution containing 3:1 nitric acid (HNO₃): sulfuric acid (H₂SO₄) for 2 h with magnetic stirring. After the acid treatment, the graphite particles were heated to 800 °C for 120 s in an open air atmosphere. After the pretreatment process, the Hummers method was used to synthesize graphite oxide. Briefly, 1 g of the pretreated graphite particles was dispersed in a solution containing 0.5 g of NaNO₃ and 23 ml of H₂SO₄ and stirred for 2 h. The obtained mixture was cooled in an ice bath before 3 g of KMnO₄ was added slowly to maintain the reaction below 20 °C. The solution was removed from the ice bath, heated to 35 °C and stirred for 30 min. To dilute the obtained mixture, 46 ml of distilled water was added; afterward, the solution was heated to 98 °C and maintained for 15 min at this temperature. After the mixture was cooled to room temperature, 140 ml of distilled water and 30 ml of H₂O₂ were added, and the mixture was stirred for 2 h. The obtained solution was filtered and washed with 100 ml of HCl; afterward, the product was washed with distilled water until the pH was between 6 and 7. The graphite oxide was dried at 50 °C in an oven.

2.2. Preparation of the GO paper

To prepare the GO paper, 30 mg of the graphite oxide particles was added to 100 ml distilled water, and the GO sheets were separated from the graphite oxide structure via ultrasonication over 2 h. After producing a homogenous dispersion of the GO sheets in the distilled water, the suspension was vacuum filtered for 2 days to form the GO paper. After vacuum filtration, the GO paper was peeled off from the polyvinylidene fluoride membrane to obtain a flexible, free-standing GO paper. The GO paper was approximately 10 µm thick. Fig. 1 shows a schematic of the GO synthesis beginning from the graphite particles.

2.3. Physical and electrochemical characterization of the GO paper

The phase constituents of the samples were determined by powder X-ray diffraction (XRD) with a Rigaku D/MAX 2000 X-ray generator and diffractometer with CuKα radiation. The diffraction patterns were collected in step scan mode and recorded in 1° (2θ) steps at 1 min per step when 5° < 2θ < 90°. Scanning electron microscopy (SEM) (Jeol 6060LV) was used to investigate the microstructure of samples.

An ECC–Air test cell (supplied from EL-Cell GmbH) was used for electrochemical characterization. The test cell was assembled in an Ar-filled glove box: the prepared GO paper was the cathode, lithium foil was the anode, 1 M LiPF₆ dissolved in tetra (ethylene glycol) dimethyl ether (TEGDME) was the electrolyte, and glass fibers were used to separate the anode and cathode. Fig. 2 shows the internal structure of ECC–Air test cell and electrode assemblies. The electrochemical performance and charge–discharge profile of the GO paper electrode was assessed from 1.0 to 4.5 V at a constant 0.01 mA cm^{−2} in ECC–Air test cell. The specific capacity of the

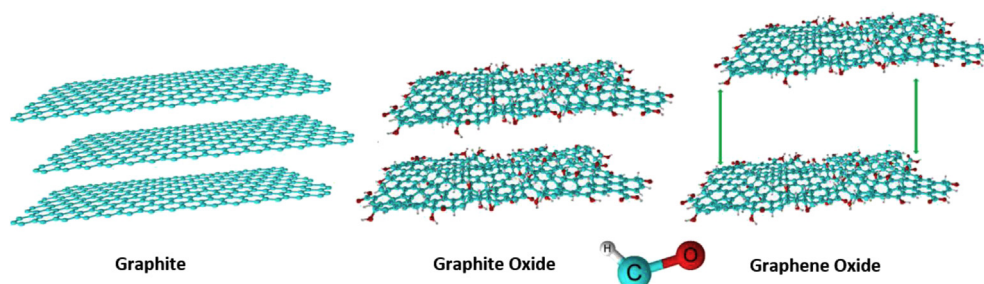


Fig. 1. Illustration of the GO synthesis from the graphite particles.

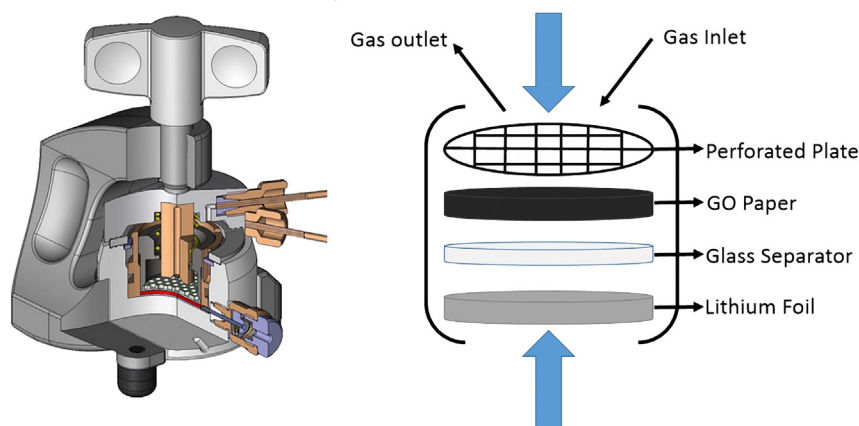


Fig. 2. ECC–Air test cell and schematic illustration of the electrode assemblies.

electrode was calculated based on the weight of the GO paper. To investigate the difference in the resistance of the cells before and after the electrochemical cycling test, electrochemical impedance spectroscopy (EIS) measurements were performed from 1000 kHz to 0.1 Hz. Moreover, to make sure about electrochemical reaction of the GO cathode with oxygen, the GO paper electrode was employed as a lithium ion battery cathode material. For this aim, CR2016 test cell was assembled in Ar-filled glove box. In the test cell, GO paper electrode was used as working electrode and lithium foil used as counter electrode. The electrode was tested at same voltage window and current density.

3. Results and discussion

3.1. Characterization of the GO paper

Fig. 3 shows the smooth, strong, and flexible nature of the 10- μm thick GO paper, which is 32 mm in diameter. Fig. 4 shows the XRD patterns of the bare flake graphite, the pretreated graphite and the final GO paper. The XRD patterns of the GO paper show a diffraction peak at $2\theta = 10.70$, indicating a larger interlayer spacing (8.1854 Å) than that of the pretreated graphite ($2\theta = 26.52$, corresponding to 3.3658 Å) due to the presence of the functional groups attached to the GO sheet surfaces and the interlamellar water trapped between the hydrophilic GO sheets [20,21]. The mean dimension of an ordered stack of GO sheets in the paper material that are oriented perpendicular to the diffracting plane can be

calculated from the width of the XRD peak using the Debye–Scherrer equation, as reported by Dikin et al. [22]. The calculated dimensions of the GO sheets revealed that 8.0628 nm corresponded to approximately 7–8 stacked GO sheets.

For further characterization, the Raman spectra of the graphite flakes and GO were studied, as shown in Fig. 5. Fig. 5 shows that the graphite particles induce a very weak peak at 1310 cm^{-1} , a strong peak at 1580 cm^{-1} and a weak peak at 2651 cm^{-1} attributed to the D, G and G' bands of the carbon, respectively. However, when the graphite structure was transformed into GO, the G and D bands appeared at 1591.35 cm^{-1} and 1306 cm^{-1} , respectively. In the Raman spectra of the GO paper, the G band was shifted toward higher Raman shifts (cm^{-1}) due to the oxygenation of graphite. The D band in GO is broadened due to the reduced size of the in-plane sp^2 domains; the reduced size is attributed to the creation of defects, vacancies and distortions of the sp^2 domains after the complete oxidation [23].

Fig. 6 shows the low and high magnification SEM images of the raw graphite flakes and the produced graphite oxide structure. As observed from Fig. 6a–b, the size of the graphite flakes ranged from 150 to 200 μm . After they are chemically oxidized, the graphite flakes show a modified configuration and particle size and are transformed into graphite oxide similar to the GO sheets, as shown in Fig. 6c–d. Fig. 7 shows surface and cross-sectional SEM images of the GO paper. The high and low magnification surface morphologies show that the GO paper was obtained by settling the GO nanosheets on top of each other (Fig. 7a and b), while the cross-

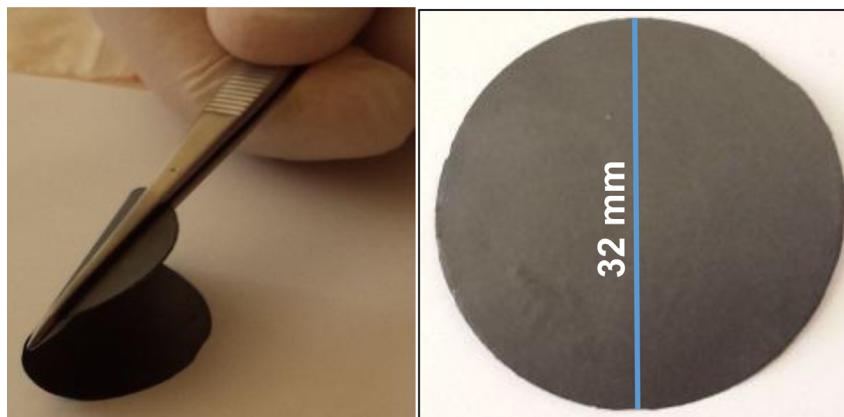


Fig. 3. Flexibility and size of the produced GO paper.

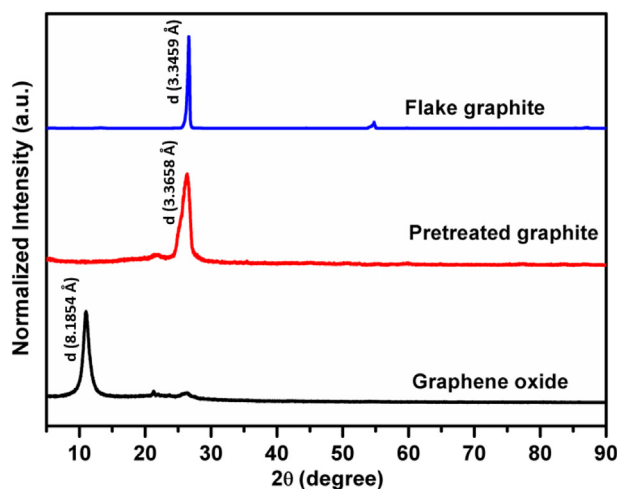


Fig. 4. Normalized XRD patterns of bare flake graphite, pretreated graphite and GO.

sectional SEM images of the GO paper show that the GO sheets were separated from the graphite oxide structure; in addition, the material has a suitable porosity for O_2 diffusion and a diffusion path for the O_2 mass transfer, improving the efficiency of the formation and decomposition of Li_2O_2 [24].

3.2. Electrochemical characterization of the GO paper

The charge–discharge profile of the GO paper electrode was obtained from the electrochemical tests carried out from 1.0 to 4.25 V in ECC–Air test cell. The charge–discharge profiles after the first, second, fifth and tenth cycles are shown in Fig. 8. The as-prepared GO paper electrode exhibited an initial discharge capacity of 1165 mAh g^{-1} and a first charge capacity of 990 mAh g^{-1} . During the discharge process, the GO paper electrode shows a plateau at approximately 2.23 V vs. Li/Li^+ due to the formation of Li_2O_2 on the surface of the GO paper. During the charging process, the plateau at approximately 3.92 V vs. Li/Li^+ indicates the decomposition of the Li_2O_2 . As it is known, almost all carbon based cathodes reduce oxygen in the voltage range of 2.5–2.0 V during discharging [25,26]. However, it is interesting to note that the reduction of the oxygen occurs between 2.23 V and 1.0 V in the GO

paper electrode during discharging as can be seen in Fig. 8. To the best of our knowledge there is only one work showing the oxygen reduction between low voltages. In this work, Kumar et al. [27] studied on long cycle life lithium–air battery and they obtained a similar oxygen reduction potential during discharging. The low reduction potential may be results in lower energy density than that of the other carbon based cathodes, but the highly reversible electrochemical reaction of the GO paper electrode make it the better cathode materials than that of other carbon based cathodes for the rechargeable $Li-O_2$ batteries. Fig. 9 exhibits charge–discharge profiles of the GO paper cathode in lithium ion battery half-cell. As can be seen from Fig. 9, the GO paper electrode shows only 46 mAh g^{-1} initial discharge capacity and 34 mAh g^{-1} first charge capacity. In the second cycle, the discharge capacity falls to 25 mAh g^{-1} and charge capacity is only 18 mAh g^{-1} . GO paper electrode shows stable capacity with further increase in cycle number. Moreover, GO paper cathode does not show any reaction plateau during charge and discharge process. As can be understood from Fig. 9, GO paper electrode in lithium ion half-cell shows very low capacity. However, Ha et al. [28] studied on reduced graphene oxide paper cathode for lithium ion batteries and they obtained better discharge capacity than that of our study, which is probably due to irreversible reactions because of Li oxidation in the case of GO used as cathode. According to study of Ha et al., reduced graphene oxide can be alternative cathode material for lithium ion batteries since interlayers of graphene behave as Li hosting regions. However, in the half-cell tests using of GO as cathode prevented Li intercalation in the voltage range, studied.

The cycling performance of the GO paper is shown in Fig. 10: the charge/discharge capacity of the GO paper decreased dramatically up to the third cycle. After three cycles, the charge/discharge capacity of the GO paper electrode stabilized, and the GO paper electrode shows a 612 mAh g^{-1} discharge capacity and a 585 mAh g^{-1} charge capacity after 10 cycles. The specific charge/discharge energy densities of the GO paper electrode are shown in Fig. 11. As can be seen from Fig. 11, the discharge energy density of the GO paper electrode is much higher than that of charge energy density due to difference of the charging and discharging reaction potentials. However, while the charge energy density of the GO paper electrode shows almost stable behavior up to 10 cycles, the discharge energy density begins to show stable energy density behavior after 6 cycles.

EIS of the GO paper electrode before and after the electrochemical cycling test (Fig. 12) and the resultant Nyquist plots were investigated. The EIS spectra fitted well on the equivalent circuit, as shown in the inset in Fig. 12. In this equivalent circuit, R_s is the ohmic resistance, which includes the electrolyte and the ionic resistance from the separator (first HF semicircle), R_{int} is the interface electronic contact resistance relevant to the resistance of the electronic contact between the GO paper and the current collector (second HF semicircle). R_{ct} is the charge-transfer resistance that corresponds to the kinetic reaction at the air electrode surface (middle frequency semicircle) and the constant phase element (CPE) attributed to the double-layer capacitance at the porous air electrode surface. The line in the low frequency region could be described by a finite length Warburg diffusion element (W_{dif}) that arose from a diffusion controlled process. The fitted resistance values are shown in Table 1. The R_e , R_{int} and R_{ct} resistances increased significantly. The increase in R_s resulted from the insulating solid discharge products generated after the electrochemical cycling test, and the increased R_{int} resistance should be attributed to increasing contact resistance between the GO paper and current collector as well as to the interfacial resistance between the electrolyte and the electrode. The increased R_{ct} can be attributed to the oxygen deficiency in the air electrode caused by the clogging of the

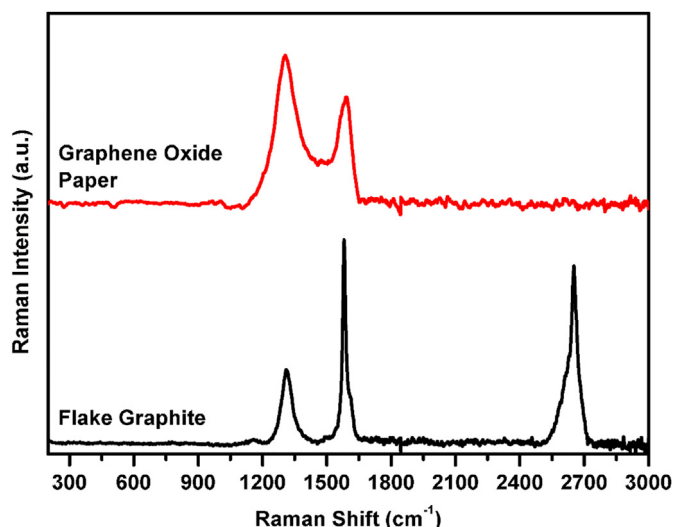


Fig. 5. Raman spectra of a) flake graphite and b) GO paper electrode.

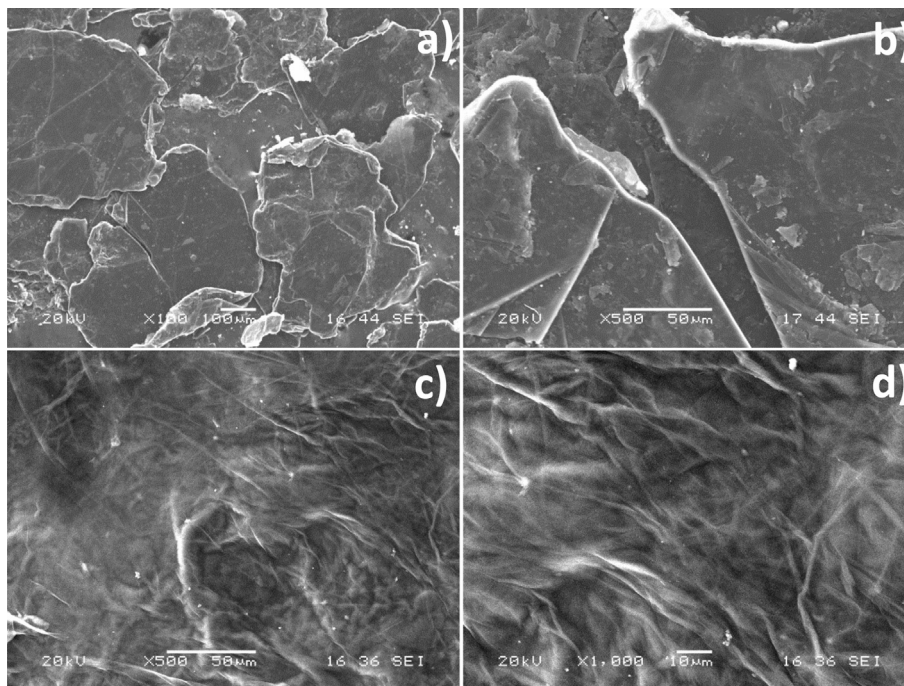


Fig. 6. Low and high magnification SEM images of flake graphite (a, b) and graphite oxide (c, d).

diffusion channels by Li_2O_2 and Li_2CO_3 on the air side after the electrochemical cycling test [10].

3.3. Characterization of the GO paper electrode after electrochemical cycling test

The XRD patterns of the GO paper electrode after 1st discharge, 1st charge and electrochemical cycling test after 10 cycles were studied, as shown in Fig. 13; Li_2CO_3 was observed at $2\theta = 32^\circ$ and 34° , and this compound was also reported by Sun et al. [29] after

discharging a graphene electrode in their study. Moreover, Li_2O_2 was detected at $2\theta = 41^\circ, 44^\circ, 52^\circ, 63^\circ$ agreeing with the work of Depart et al. [30]. As can be seen from Fig. 13, the Li_2O_2 and LiCO_3 compounds deposited on the surface of GO paper cathode after discharging. But, Li_2O_2 and LiCO_3 peaks almost disappeared after charging, which shows highly reversible reaction of the GO paper electrode [3,30]. However, the XRD patterns of the GO paper electrode after 10 charge/discharge cycles showed the Li_2O_2 and LiCO_3 compounds in the GO paper electrode. As shown by the electrochemical performance of the GO paper electrode in Figs. 8 and 10,

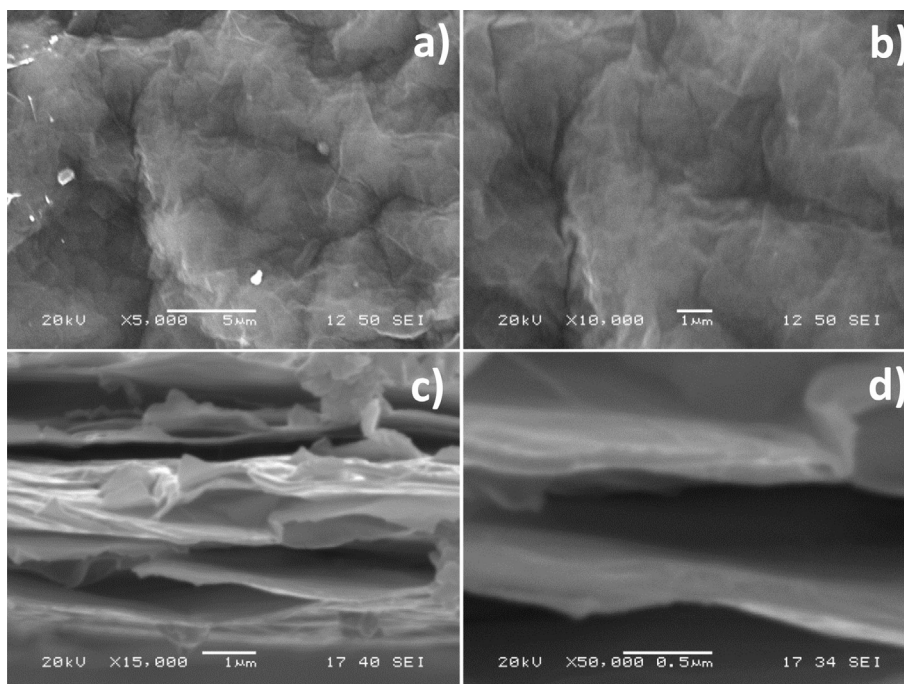


Fig. 7. Low and high magnification surface (a, b) and cross-sectional (c, d) SEM images of GO paper.

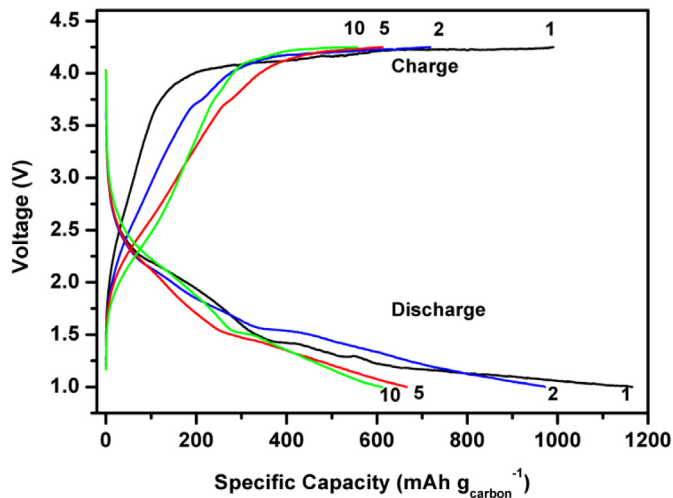


Fig. 8. Charge–discharge profile of GO paper in ECC–Air test cell.

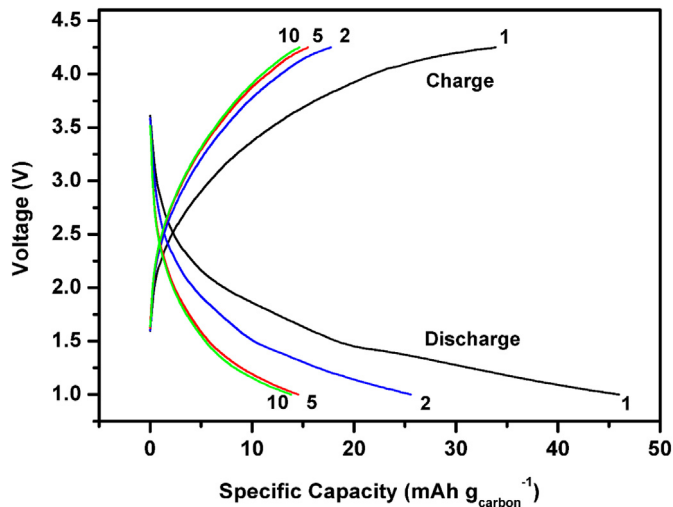


Fig. 9. Charge–discharge capacity of GO paper cathode in CR2016 cell.

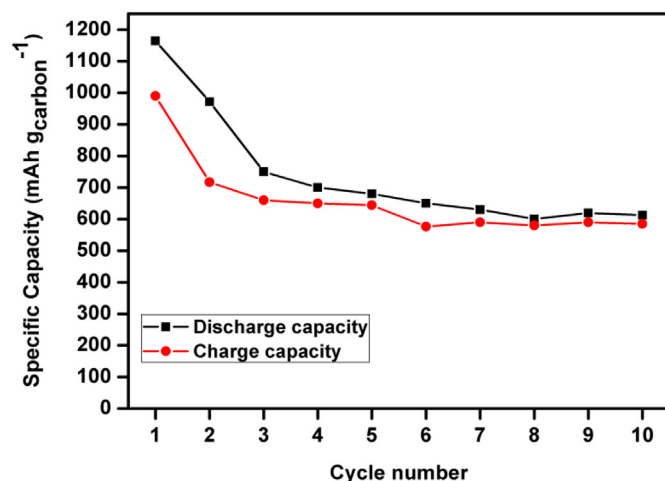


Fig. 10. Cyclic performance of the GO paper until tenth cycle.

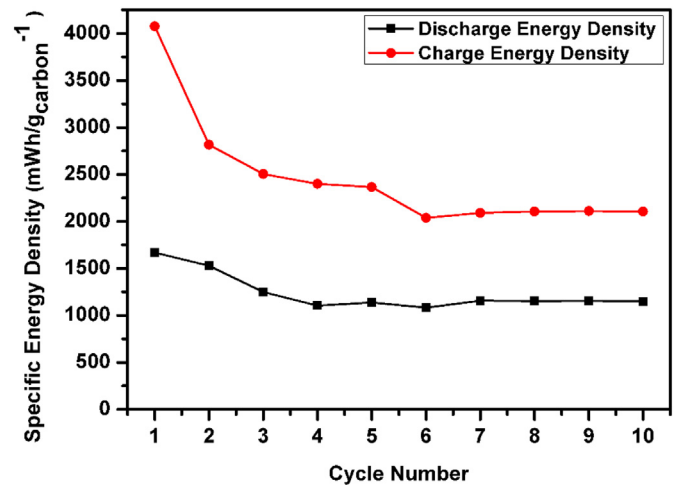


Fig. 11. Specific charge/discharge energy density of the GO paper until tenth cycle.

the GO paper electrode loses its capacity over three cycles. Therefore, some of the obtained Li_2O_2 and Li_2CO_3 compounds most likely precipitate in the porous structure of the GO paper, blocking further oxygen intake and decreasing the capacity fading for initial cycles [3]. Moreover, the XRD patterns of the as-prepared GO paper showed 2θ values of 10.7° that shifted to 25.6° after the electrochemical cycling test. This result shows that the as-prepared GO paper transforms into a graphene structure after the electrochemical cycling test. To verify this result, Raman spectroscopy was carried out on this electrode, as shown in Fig. 14; the Raman spectrum of the GO electrode after 10 cycles is significantly different from the spectrum of the fresh GO paper electrode (shown with Fig. 5). After the electrochemical cycling test of the GO paper electrode, the G band is shifted toward lower Raman shift values (1590 cm^{-1}) and becomes weaker. The D band becomes narrow and increases in intensity; the full width at half maximum (FWHM) of the D peak decreases. These phenomena can be observed from the reduced GO or/and graphene in the literature. The increased intensity and decreased FWHM of the D peak relative to that of the fresh GO electrode were caused by the increased average size of the sp^2 clusters [23,31]. The XRD and Raman spectra of the GO paper

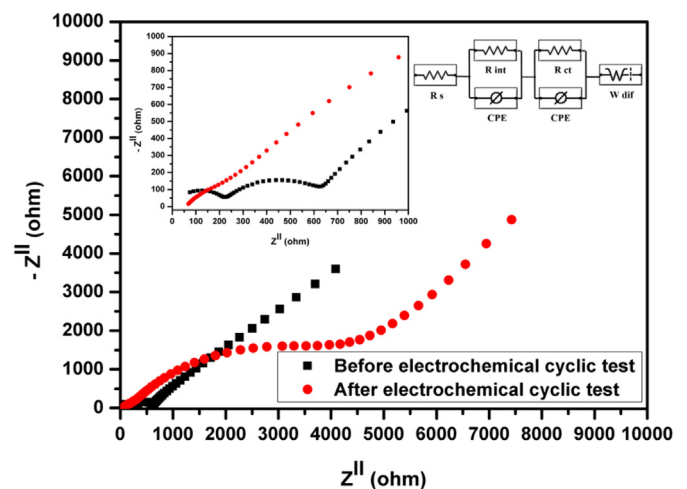
Fig. 12. Nyquist plots of the before and after electrochemical cycling GO paper electrode. Inset figures represent low Z' (ohm) values of nyquist plot and equivalent circuit fitted on the nyquist plots.

Table 1
Fitted resistance values in the equivalent electric circuit.

Parameter	R_s (Ω)	R_{int} (Ω)	R_{ct} (Ω)
Before electrochemical cycling test	80	221	232
After electrochemical cycling test	83	246	2795

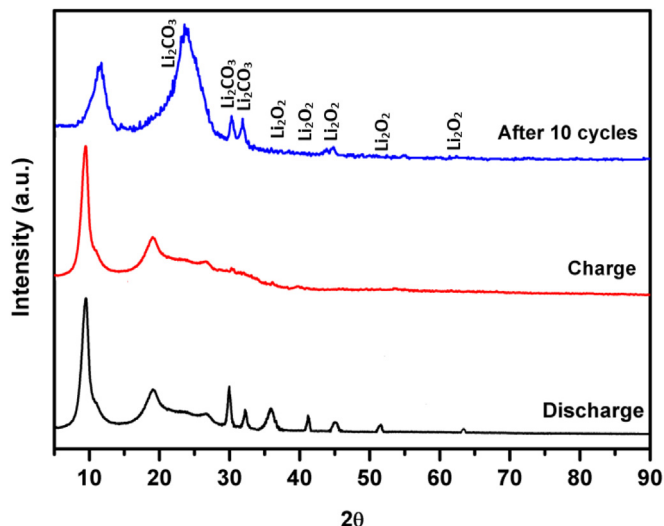


Fig. 13. XRD patterns of the GO paper electrode after discharge, after charge and after 10 electrochemical cycling test.

electrode indicate that the GO structure in the electrode was reduced to graphene during electrochemical cycling. The electrochemical test in this work was interrupted after charging. The Li–air batteries reduced oxygen with lithium ions during discharge to form Li_2O or Li_2O_2 ; these oxides are electrochemically decomposed to form lithium ions and oxygen during the charging process [32]. The decomposition of the lithium oxides to form metallic lithium should explain why GO reduction is most likely mediated by metallic Li ions. This mechanism implies that using GO nanosheets does not significantly decrease the occurrence of reduced graphene nanosheets. Because the carbon active materials use oxygen catalysis in the Li–air batteries, pure graphene should be

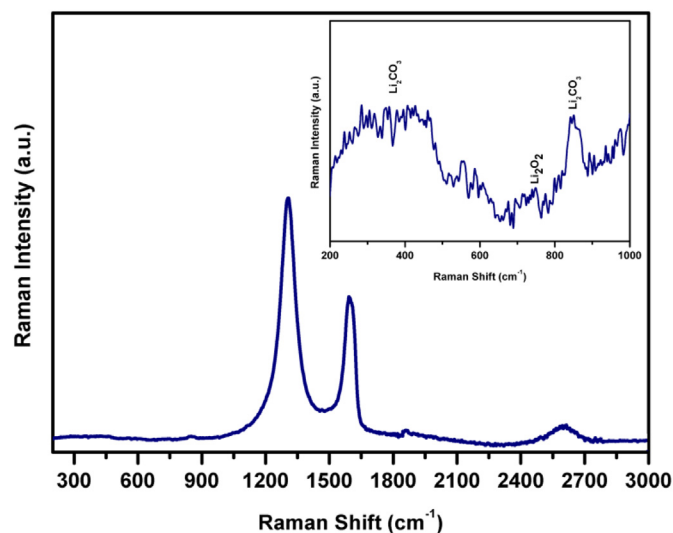


Fig. 14. Raman spectra of GO paper electrode after electrochemical cyclic test and inset figure shows low Raman shift (cm^{-1}) values of the figure.

oxidized during the discharge process. Therefore, using GO will provide the same electrochemical mechanisms as pure graphene nanosheets, indicating that the specific capacity values obtained in this study should possess higher capacities because GO was used as the active material. Due to the GO reduction, the real capacities should be somewhat higher than the measured capacity values.

4. Conclusions

A GO paper was produced using a vacuum filtration technique and employed as the cathode material for Li– O_2 batteries. The GO paper exhibited a 612 mAh g^{-1} discharge capacity and a 585 mAh g^{-1} charge capacity after 10 cycles. After the electrochemical cycling test, Li_2O_2 and Li_2CO_3 deposited on the GO paper electrode. R_s , R_{int} and R_{ct} values increased after the electrochemical cycling test due to the insulating solid discharge products, the increased contact resistance between the GO paper and current collector and the clogging of diffusion channels by the Li_2O_2 and Li_2CO_3 products on the air side. The study is also proved the GO paper transforms into graphene during the electrochemical cycling test. The unique structure of the GO paper provided enough porosity for O_2 diffusion; the diffusion path for the O_2 mass transfer improved the efficiency of the formation and decomposition of Li_2O_2 . The GO paper might be a promising cathodic material for lithium–air batteries due to its high reversible capacity. The study showed the GO was obtained to be reduced during the charging process and this reduction was attributed to the reversibility of the graphene and GO formation during the charging and discharging processes.

Acknowledgments

This research has received funding from the Seventh Framework Programme FP7/2007–2013 (Project STABLE – Stable high-capacity lithium–Air Batteries with Long cycle life for Electric cars) under grant agreement 314508.

References

- [1] F. Cheng, J. Chen, *Nat. Chem.* 4 (2012) 962–963.
- [2] Y. Wang, *Electrochim. Acta* 75 (2012) 239–246.
- [3] A.K. Thapa, Y. Hidaka, H. Hagiwara, S. Ida, T. Ishihara, *J. Electrochem. Soc.* 158 (2011) A1483–A1489.
- [4] Y. Lu, Z. Wen, J. Jin, Y. Cui, M. Wu, S. Sun, *J. Solid State Electrochem.* 16 (2012) 1863–1868.
- [5] Y. Yang, Q. Sun, Y.S. Li, H. Li, Z.F. Fu, *J. Electrochem. Soc.* 158 (2011) B1211–B1216.
- [6] H. Minowa, M. Hayashi, K. Hayashi, R. Kobayashi, K. Takahashi, *J. Power Sources* 244 (2013) 17–22.
- [7] H.G. Jung, J. Hassoun, J.B. Park, Y.K. Sun, B. Scrosati, *Nat. Chem.* 4 (2012) 579–585.
- [8] C.K. Park, S.B. Park, S.Y. Lee, H. Lee, H. Jang, W.I. Cho, *Bull. Korean Chem. Soc.* 31 (2010) 3221–3224.
- [9] T.H. Yoon, Y.J. Park, *Nanoscale Res. Lett.* 7 (2012) 28.
- [10] G.Q. Zhang, J.P. Zheng, R. Liang, C. Zhang, B. Wang, M. Hendrickson, E.J. Plichta, *J. Electrochem. Soc.* 157 (2010) A953–A956.
- [11] Y. Li, K. Huang, Y. Xing, *Electrochim. Acta* 81 (2012) 20–24.
- [12] M. Mirzaei, J.H. Peter, *Electrochim. Acta* 54 (2009) 7444–7451.
- [13] Y. Li, J. Wang, X. Li, D. Geng, M.N. Banis, R. Li, X. Sun, *Electrochem. Commun.* 18 (2012) 12–15.
- [14] Z.L. Wang, D. Xu, J.J. Xu, L.L. Zhang, X.B. Zhang, *Adv. Funct. Mater.* 22 (2012) 3699–3705.
- [15] Y. Xu, W. Hong, H. Bai, C. Li, G. Shi, *Carbon* 47 (2009) 3538–3543.
- [16] G. Wang, B. Wang, J. Park, J. Yang, X. Shen, J. Yao, *Carbon* 47 (2009) 68–72.
- [17] Ravikumar, K. Scott, *Chem. Commun.* 48 (2012) 5584–5586.
- [18] X. Sun, Z. Liu, K. Welscher, J.T. Robinson, A. Goodwin, S. Zaric, H. Dai, *Nano Res.* 1 (2008) 203–212.
- [19] W.S. Hummers, R.E. Offeman, *J. Am. Chem. Soc.* 80 (1958) 1339–1339.
- [20] V.H. Pham, T.V. Cuong, S.H. Hur, E. Oh, E.J. Kim, E.W. Shin, J.S. Chung, *J. Mater. Chem.* 21 (2011) 3371–3377.
- [21] C. Valles, J.D. Nunez, A.M. Benito, W.K. Maser, *Carbon* 50 (2012) 835–844.
- [22] D.A. Dikin, S. Stankovich, E.J. Zimney, R.D. Piner, G.H.B. Dommett, G. Evmenenko, S.B.T. Nguyen, R.S. Ruoff, *Nature* 448 (2007) 457–460.

- [23] K. Krishnamoorthy, G.S. Kim, S.J. Kim, *Ultrason. Sonochem.* 20 (2013) 644–649.
- [24] Y. Li, J. Wang, X. Li, D. Geng, R. Li, X. Sun, *Chem. Commun.* 47 (2011) 9438–9440.
- [25] J. Wang, Y. Li, X. Sun, *Nano Energy* 2 (2013) 443–467.
- [26] A. Kraytsberg, Y.E. Eli, *J. Power Sources* 196 (2011) 886–893.
- [27] B. Kumar, J. Kumar, R. Leese, J.P. Fellner, S.J. Rodrigues, K.M. Abraham, *J. Electrochem. Soc.* 157 (2010) A50–A54.
- [28] S.H. Ha, Y.S. Jeong, Y.J. Lee, *ACS Appl. Mater. Interfaces* 5 (2013) 12295–12303.
- [29] B. Sun, B. Wang, D. Su, L. Xiao, H. Ahn, G. Wang, *Carbon* 50 (2011) 727–733.
- [30] A. Debart, J. Bao, G. Armstrong, P.G. Bruce, *J. Power Sources* 174 (2007) 1177–1182.
- [31] G. Wang, J. Yang, J. Park, X. Gou, B. Wang, H. Liu, J. Yao, *J. Phys. Chem. C* 112 (2008) 8192–8195.
- [32] T. Ogasawara, A. Debart, M. Holzapfel, P. Novak, P.G. Bruce, *J. Am. Chem. Soc.* 128 (2006) 1390–1393.